Investigation of Electroosmotic Flow in Various Microfluidic Structures using a Micro Programmable Object Navigation Gadget (μ-PONG) Instrumentation System

Patrick Diggins
Advisors: Philip Samson and John P. Wikswo

Senior Honors Thesis
Spring 2010

Table of Contents

Background and Significance:

Enclosed microfluidic devices provide excellent systems for the study of biological processes such as cell-cell, paracrine, and autocrine signaling systems. By minimizing the fluid volume within the chambers, microfluidic devices diminish the dilution of secreted products which makes the detection of the secreted products a more straightforward task. In addition, for many biological applications microfluidic devices are superior to traditional large-format Petri dish cell culture systems because the small volumes contained within the small microfluidic devices more closely recreate the cell volume to extracellular fluid volume ratios of *in vivo* tissue environments.

A major design problem associated with the construction of microfluidic devices for biological research is the need to provide well-controlled fluidic transportation for cells, the nutrients that the cells need, and waste removal. In particular, for long term biological experiments (lasting for days) with living cells, pumps are needed to transport nutrients through the microfluidic channels into the small chambers in which cells reside. In many cases, the pumps need to produce low flow rates which should not disrupt the diffusion gradients which surround the cells or cause shear stress which can cause damage to the cells. Most precision syringe pumps which can accurately provide low flow rates are expensive and constitute a barrier to experiment design. Electroosmotic pumps could potentially provide a valuable alternative as a low volume flow rate pumping system for many types of microfluidic devices.

Objective:

The goal of this project is to develop a poly(dimethylsiloxane) (PDMS) microfluidic device that incorporates both electroosmotic flow and pressure driven flow. The device is designed to increase the relative strength of the electroosmotic flow (EOF) component of the total flow through the use of an array of small volume parallel pumping channels which provide higher passive resistance to pressure driven flow than a larger volume single-channel EOF pump. Using a novel microfluidic instrumentation device which we call the “Micro Programmable Object Navigation Gadget” (μ-PONG), we investigate how different properties and geometries of the device affect the EOF rate. The primary investigation is to compare the flow rates for different dimensions of channels. An additional goal is to demonstrate that fluid flow driven by a small hydraulic pressure head can be completely canceled by an user initiated EOF in the pumping channels which are incorporated into a microfluidic device. The ability to modulate the flow and to create “stop flow” conditions in microfluidic devices is also important for biological research.

Introduction:

Electroosmotic flow is based on the phenomenon of electroosmosis which was first discovered by F.F. Reuss in 1809[1], and then theoretically analyzed in terms of an electric double layer model by Helmholtz[2] and later Smoluchowski.[3] In electroosmosis, the flow of an uncharged fluid enclosed in a channel that is bounded by walls which contain fixed surface charges can be controlled by applying an external electric field. The electric double layer (EDL) is created when regions of localized charge immobilized on the surface attract oppositely charged ions and particles from the fluid. The EDL theory provides the foundation for electroosmotic pumps (EOPs). EOPs can create flows that have easily controlled magnitude and direction; do not require any moving parts; require only standard microfabrication techniques; and can be integrated into lab-on-chip (LOC) devices.[4]

PDMS is commonly used in experiments using EOF, especially in biological experiments concerning the manipulation of biomolecules[5] and cells.[6] The benefits of using PDMS in biological experiments are that PDMS is nontoxic to cells, optically clear, and permeable to

gases.[7] In addition, PDMS can be bonded to a variety of surfaces including other PDMS and glass surfaces through the process of surface oxidation. The oxidation creates Si-O localized charge regions on the surface, which also increases the surface hydrophilicity.[8] The hydrophilic, polar surface with a localized charge distribution is ideal for EOF.

Theoretical Discussion:

When a fluid is brought into contact with a charged surface, ions of opposite charge from the fluid are attracted to the charged surface regions to form the EDL. The surface charges are stationary because of their bonds with other atoms in the solid and thus do not move even when an electric field is applied parallel to the surface. On the other hand, the ions from the fluid that are part of the EDL will move along a path parallel to the surface when an external electric field is applied. The moving ions near the surface drag the bulk fluid atoms with them. As a result, the entire fluid is dragged in one direction, regardless of the charges of the atoms in the bulk fluid. The process is illustrated in Figure 1.

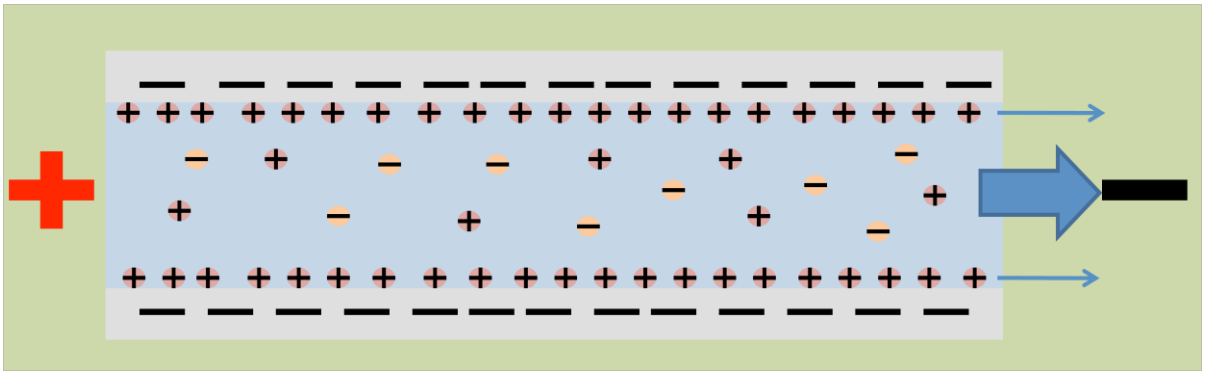

Figure 1. Illustration of electroosmotic flow (EOF) in a microfluidic channel bounded by solid surfaces containg localized negative chanrges. Cations from the fluid are attracted to the negative surface charges to form the EDL. The fluid cations in the EDL move in the direction of the negative potential which is created by a set of electrodes. The cations drag the rest of the fluid in the same direction.

The EOF can be characterized by the electroosmotic mobility, μ_{eo} which is defined by

$$\mu_{eo} = \frac{\epsilon\zeta}{\eta} \tag{1}$$

where ε is permittivity of the solution, ζ is the Zeta potential at the surface, and η is the viscosity of the solution.[9,10] Based on the flow velocity, v_{eo}, can then be written as

$$v_{eo} = \mu_{eo} E \tag{2}$$

where E is the electric field.[5,6,]

For square channels in an open system of height a and length L where $L>>a$, the electric field can be written as

$$E = \frac{V}{L}. \tag{3}$$

where *V* is the potential difference between the two ends of the channel. The following derivation for the EOF follows the derivation shown in Wang *et. al*.[4] and Lui *et. al.*[11] except to replace the rectangular channels they used with square channels.

In this situation, the velocity can be written as

$$v_{eo} = \frac{\varepsilon \zeta V}{4\pi\eta L}. \tag{4}$$

As this equation shows, EOF is a plug flow, so the velocity is not dependent on the transverse location within the channel. Thus the flow rate, Q_{eo}, inside a square channel is

$$Q_{eo} = \frac{\varepsilon \zeta V a^2}{4\pi\eta L}. \tag{5}$$

If n channels are assembled in parallel, the total flow rate is

$$Q_{eo} = \frac{n\varepsilon \zeta V a^2}{4\pi\eta L}. \tag{6}$$

Thus the flow rate is proportional to voltage, the number of channels, and the cross sectional area of the channel. The previous equations dealt only with EOF in a long, open channel, but in fluidic networks, a backpressure is created as the fluid flows. The back pressure in a device with length *L'* and diameter *d* can be described using the Hagen-Poiseuille equation

$$\Delta p = \frac{-128\eta L' Q}{\pi d^4}. \tag{7}$$

In calculating the backpressure, the device can by represented by an equivalent channel of length *L'* and diameter *d*. The flow rate caused by the back pressure in the pumping channels is equal to the pressure difference divided by the hydrodynamic resistance of the channels.

The flow through microfluidic channels can be explained using a circuit analog. For a rectangular channel, the conductance, *G*, is described by

$$G = \frac{1}{R} = \frac{4\left(w/2\right)\left(h/2\right)^3}{3\eta L}\left(1 - \frac{192\left(h/2\right)}{\pi^5\left(w/2\right)} \sum_{j=1,3,5\ldots}^{inf} \frac{tanh\left(i\pi w/2h\right)}{j^5}\right). \tag{8}$$

For a square channel, the resistance can be simplified to

$$R = \frac{28.453\eta L}{a^4}. \tag{9}$$

For a group of *n* channels with the same dimensions in parallel, the equivalent resistance is given by

$$\frac{1}{R_{eq}} = \frac{1}{R} + \frac{1}{R} + \cdots = \frac{n}{R}. \tag{10}$$

Thus equivalent resistance is

$$R_{eq} = \frac{R}{n} = \frac{28.453\eta L}{na^4}. \tag{11}$$

For any pressure drop and resistance, the flow rate through a channel is[12]

$$Q = \frac{\Delta p}{R}. \tag{12}$$

Thus the back flow, Q_b, through the channels is

$$Q_b = \frac{-na^4\Delta p}{28.453\eta L}. \tag{13}$$

Hence the back flow is related to the forward flow, Q_c, by combining Eqs. 7 and 12

$$Q_b = \frac{4.4986nL'a^4}{\pi d^4 L} Q_c. \tag{14}$$

When assuming incompressibility and continuity hypothesis for liquids, we find that Q_{eo} becomes

$$Q_{eo} = Q_c + Q_b. \tag{15}$$

Therefore, the forward flow can be expressed by combining Eqs. 6, 14, and 15 to obtain

$$Q_c = \frac{n\epsilon\zeta d^4 V a^2}{4\eta(\pi d^4 L + 4.4986nL'a^4)}. \tag{16}$$

The efficiency of the pump, β, which is the ratio of the forward flow, Q_c, to the total flow, Q_{eo}, becomes

$$\beta = \frac{\pi d^4 L}{(\pi d^4 L + 4.4986nL'a^4)}. \tag{17}$$

Eqs. 14 and 15 show that the forward flow portion of the EOF increases as the number of channels, the applied voltage, or the cross-sectional area of the channels increases. On the other hand, the efficiency of the device decreases as the number of channels or the cross-sectional area increases. Thus the net flow can actually decrease as the back pressure becomes larger.

The previous equations are for an EOF pump where the EOF is the only flow in the channel. In many devices, there is also an external pressure differential which creates a pressure flow. The pressure flow, Q_p and the EOF can be superimposed to find the total flow through the device

$$Q_{tot} = Q_{eo} + Q_p. \tag{18}$$

Methods:

The Microfluidic Device Design

A block-diagram of the microfluidic device used in our experiments is shown in Figure 2. The device was primarily designed to provide robust control over the magnitude and direction of

the flow. In order to maximize the total EOF, the design incorporates a series of square pumping channels positioned in parallel with each other. Two cross sectional dimensions of parallel pumping channels were used in experiments: 15 μm x 15 μm and 32 μm x 32 μm. Pumping channels are connected to two wells. Electrodes are placed in the two wells. A larger channel is connected to one of the wells. This channel is called the observation channel and is where the flow rate is measured. A third well is connected to the end of the observation channel. This well provides an opening in which to input material into the device that can be connected to the observation channel without being affected by the electric field created by the electrodes.

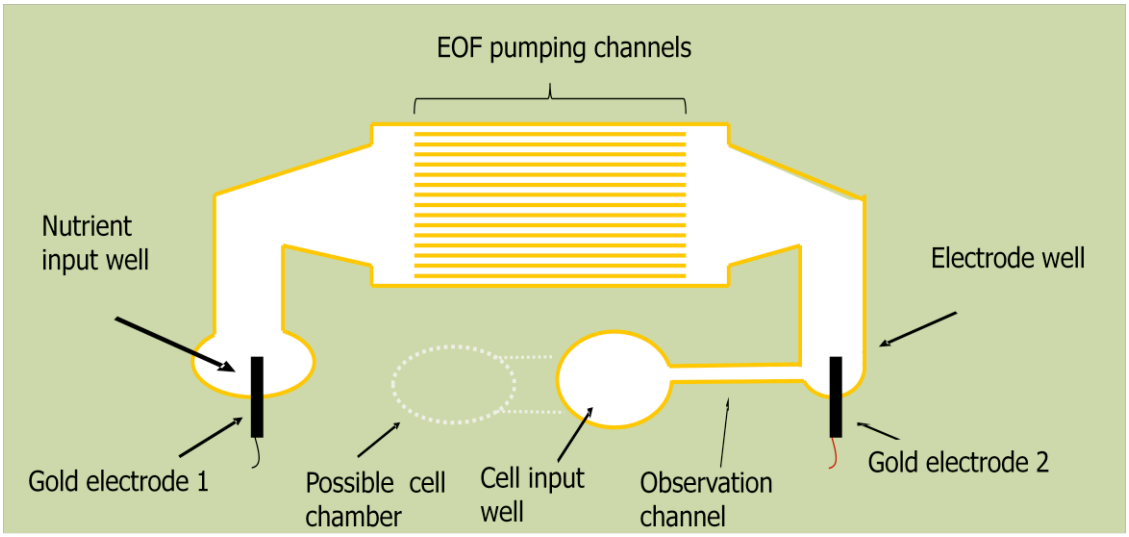

Figure 2. Schematic of microfluidic device. The input well on the left also contains the left electrode. The width and height of the pumping channels depend on the device. It would be possible to add additional channels to the device so that it could be used in different experiments.

The well between the pumping channels and the observation channel, termed the electrode well, is smaller than the other two wells. The electrode well enables an electrode to be placed into the middle of the device. Since the observation channel is not in the circuit between the electrodes, it is not directly affected by EOF. This reduces the effects of an electric field in the channel and whatever it contains. Thus, in the observation channel there is only a pressure flow which is determined by the summed contributions of the external pressure difference and the EOF.

Initial experiments showed that the smaller diameter electrode wells work better than wells with a larger diameter. After the device is fabricated and filled with water, a cap is placed over the central electrode well to prevent fluid from escaping and to insure that aggregate flows will be accurately registered in the observation channel.

Pump Design

The EOF pumping channels for both designs are spaced with 50% spatial duty cycle. Thus, there is a greater spacing between larger channels than for smaller ones. The reason for this design is to keep the total surface area in the channels equivalent regardless of the cross-sectional area as shown in Figure 3.

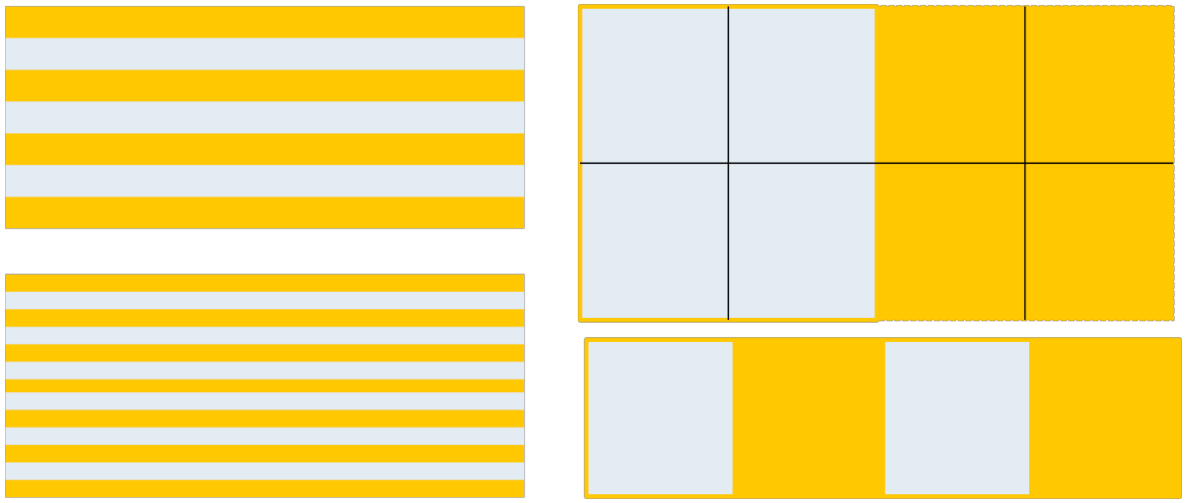

Figure 3: Surface area for different dimensions. Yellow represents PDMS while gray represents the fluid inside the channel. **Left:** The pictures represent a top-down view of the pumping channels for two different channel widths. The separation between the pumping channels is equal to the width of the pumping channels for both sizes of channels. This causes the total surface area of the channels to remain constant. **Right:** The pictures represent the cross-sectional area of the two types of channels of different dimensions. Note that the array of large channels has twice the cross sectional area as the array of small channels.

For our particular type of design, the total number of channels, *n*, equals

$$n = \frac{W}{2a} \tag{19}$$

where *W* is the total width of the pumping channel area and a is the width of an individual channel. Now the cross sectional area (*SC*) of the pumping channels is equal to

$$SC = na^2 = \frac{W}{2a}a^2 = \frac{Wa}{2} \tag{20}$$

while the surface area of the pumping channels is equal to

$$SA = nL(4a) = \frac{W}{2a}L(4a) = 2LW. \tag{21}$$

Therefore for this pump array geometry, the total surface area of the pumping channels is constant, but the cross-sectional area increases linearly with the width of the channels. For the devices, the pumping channel region has a length of 1cm and a total width of 1cm, so from Eq. 20, the *SA* equals 2 cm^2. The cross-sectional area is equal to 75000 μm^2 for the 15 μm channels and 160000 μm^2 for the 32 μm channels.

Circuit Analog

The device can also be viewed as a circuit (Figure 4). The two end wells of the device can be viewed as capacitors. The pumping channels are related to a current source with an internal resistance. The observation channel is analogous to a resistor. In addition, the rest of the channels also have a resistance, but the dimensions of these channels are much greater and so their resistance is negligible compared to the internal resistance of the pumping channels and the resistance of the observation channel.

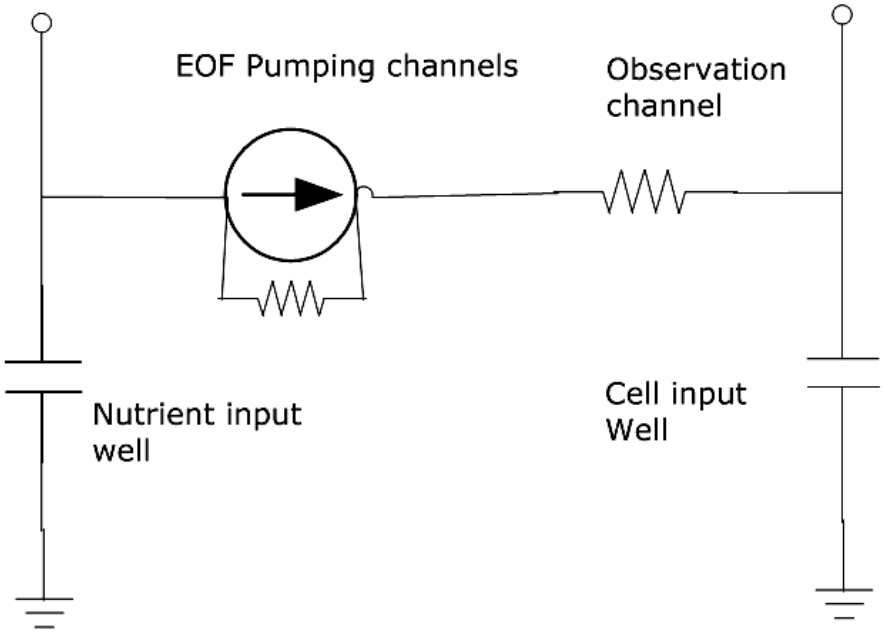

Figure 4. An equivalent circuit diagram of the microfluidic device. The two end wells act as capacitors. The pumping channels are represented by a current source in parallel with a resistor. The observation channel acts as a resistor in series with the pumping channels.

Using Eq. 10, the resistances of the devices were calculated. For the 15 μm channels, the resistance of the pumping channels was 1.69×10^{-5} Pa-s/μm^3. For the 32 μm channels, the resistance was1.74×10^{-6} Pa-s/μm^3. The resistance of the observation channel is found using Eq. 8 with the summation taken to 5 elements. For the 15 μm device, the resistance of the observation channel is 3.33×10^{-5} Pa-s/μm^3. For the 32 μm device, the resistance is 4.60×10^{-5} Pa-s/μm^3.

Fabrication of PDMS Devices

The PDMS devices were fabricated using photolithography to create master molds and standard soft lithography microfabrication techniques to create the PDMS microchannels from the mold (Figure 5). The device design is first created in a drawing program (AutoCad) which is then transferred to a mask. For these experiments, the mask had two parts, one part for the pumping channels, and the other part for the rest of the device. SU-8 photoresist was spun onto a silicon wafer. The depth of the photoresist is determined by the viscosity of the photoresist and the angular velocity of the wafer after the photoresist has been poured. The photoresist is exposed to ultraviolet (UV) light through the mask for the pumping channels. The exposed areas of the photoresist polymer become crosslinked. The wafer is placed on a hot plate so that the

cured photoresist can harden. The process is then repeated a second time with the mask for the rest of the device. Then the unexposed photoresist is dissolved using a solvent which does not remove the photo-crosslinked cured regions of the pattern. The use of repeated lithography enables the two parts of the device to have different heights.

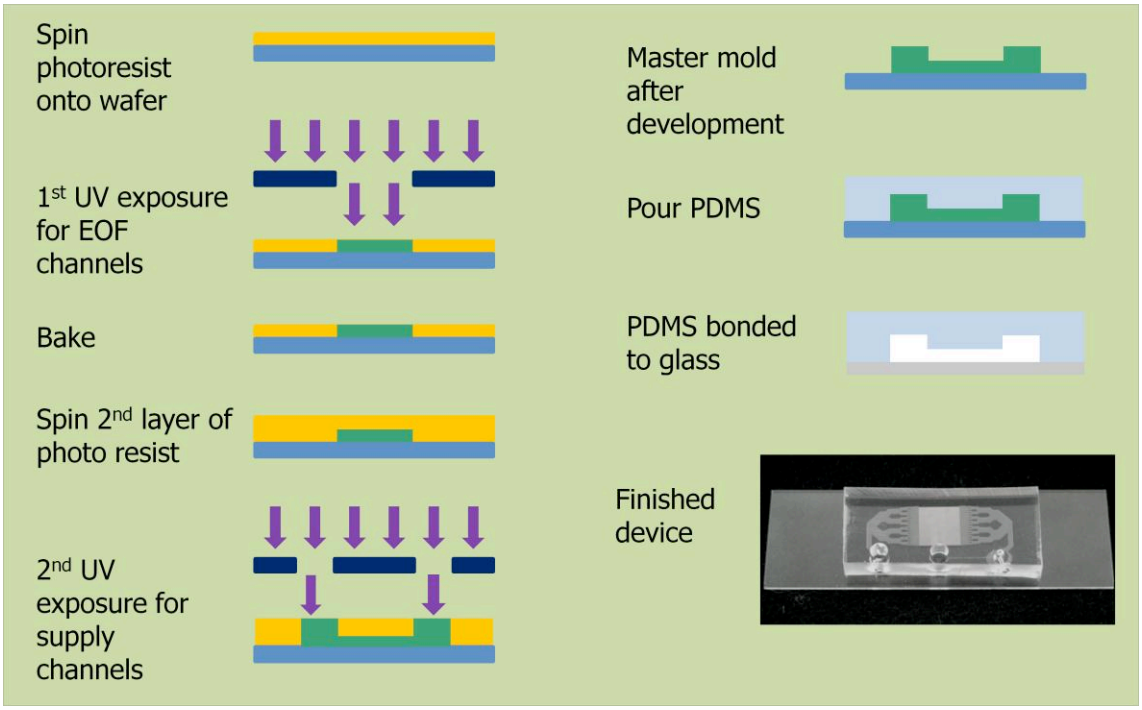

Figure 5. Manufacturing of microfluidic devices. The figure shows a schematic of the photolithography and microfabrication of PDMS channels. The process of photolithography is done twice (once for the pumping channels and again for the rest of the device) in order to create a master mold in which the pumping channels will be a different height than the rest of the device.

Once the master has been made, the PDMS device is created using a two stage pour process in order to create a tight fitting conformal socket into which the reusable gold plated electrodes used with μPONG will fit. PDMS fabrication begins by combining uncured PDMS (Sylgard 184 Silicone Elastomer Base) with a cross linking agent (Sylgard 184 Silicone Elastomer Curing Agent) to produce a viscous liquid that becomes solid on application of heat. First, around 10 mm of PDMS mix are poured over the mold. The device is then placed in a vacuum in order to degas the PDMS. Once all bubbles around the device are degassed, the device is placed in an oven set between 55 and 65 C^{o}. The device is kept in the oven for 25 to 30 minutes, so that the PDMS has partially solidified and is rigid enough to support the weight of an electrode. Then dummy electrodes are placed on the PDMS over the electrode well and the opposite input well. These dummy electrodes serve as molds to create sockets into which the actual μ-PONG electrodes will be placed. If the PDMS is not baked long enough, the electrodes will sink to the bottom of the PDMS, and if it is baked too long, there is an increased chance for large bubbles deforming the device (Figure 6). After the electrodes have been placed in the device, a second layer of PDMS is poured on top of the first layer. The device is then degassed and placed back in the oven overnight.

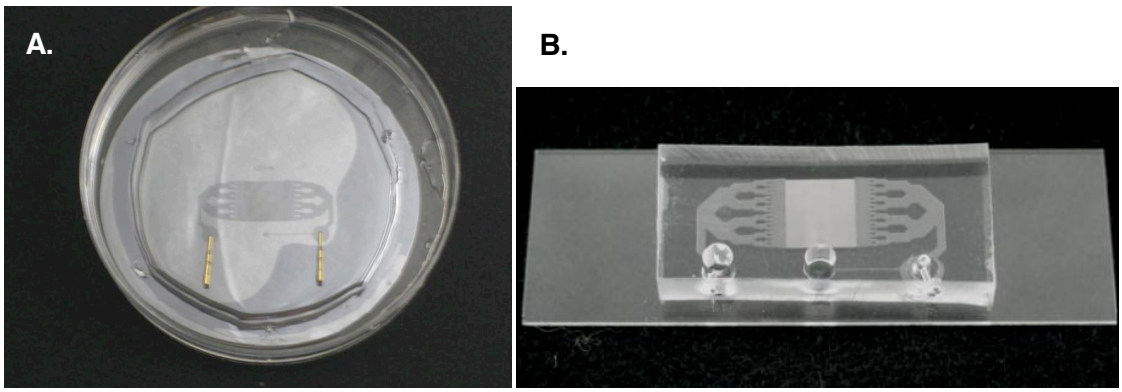

Figure 6: Images of PDMS devices. A) The picture shows a device with a deformation at the interface between the mold and the device that formed after the second layer of PDMS was poured. The effect only occurs when the second layer is poured after the first layer has been allowed to harden past a certain point (normally 25 minutes). It is believed that the deformation forms while the device is in a vacuum during the degassing stage. **B)** The picture shows a device that has been punched and irreversibly bonded to a glass slide.

Once the device is removed from the oven, the PDMS is pulled off the wafer and the dummy electrodes are removed from the PDMS. The three wells are punched into their respective positions and then the device is placed in a plasma cleaner (Harrick Plasma PDC-001) for 30 seconds and then irreversibly bonded to the device. Distilled water is then immediately poured into the device to maintain the hydrophobic nature of the surface of the oxidized PDMS. Once the device is prepared and the regular electrodes are inserted, it is connected to the μ-PONG system.

μ-PONG

The μ-PONG system modulates the voltage at the ends of the device through two electrodes that are connected to an external voltage switching circuit. The circuit and a data acquisition (DAQ) board are connected to a computer. A camera that is connected to a microscope records the image of a bead and transmits the image to the computer. A program (PONG 2.5.2) interprets the data and modulates the voltage through the electrodes. Figure 7 shows the schematic of the μ-PONG system.

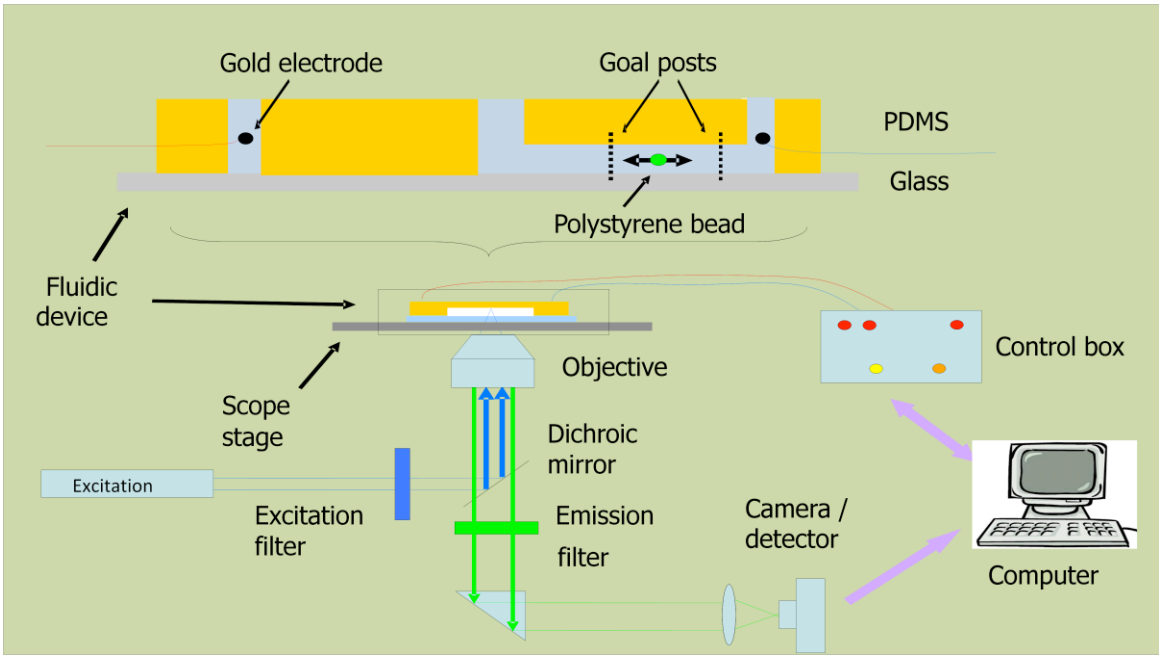

Figure 7. Schematic of *μ*-PONG. The device is placed on the microscope and the two gold electrodes that are connected to the control box are placed in the openings that the dummy electrodes created. A blue light excites the fluorescent bead which is imaged by a camera using fluorescence microscopy. The camera is connected to a computer which runs the PONG program. The program analyzes and displays the image and then communicates necessary commands to the control box. The control box contains the DAQ board and the external voltage switching circuit. The circuit controls the voltage through the electrodes. When the PONG program is in automatic mode, the computer will switch the voltage across the electrodes when it detects that the bead has entered a virtual "goalpost" as defined by the user. While in automatic mode, the bead will remain in continuous motion, trapped between the two goalposts.

The external voltage circuit contains a computer controlled National Instruments USB-6009 digital-to-analog device which can produce output voltages in the range from 0 to 5 volts. The external circuit generates a positive and negative voltage equal to the input voltage from the USB-6009 device and then amplifies the voltage by a factor of 1.83. An additional voltage channel controls the direction of the potential difference between the two electrodes.

The camera is a Mightex BCE_BG05-001 global shutter camera. In a global shutter camera, all the CCD pixels in the camera are reset at the same time before the next image is taken. Each pixel begins accumulating charge from photons at the same time and for the same duration of time. This reduces the effect of motion blurring compared to rolling shutter cameras.

The beads used in the experiments were carboxylated fluorescent polystyrene beads with diameters of 3 μm (Polysciences, Inc. Fluoresbrite YG microspheres, CV = 5%).

The computer program views the images from the camera and displays the video in real time on the computer screen. The user defines two areas called virtual "goalposts" at opposite ends of the channel in the video. The program analyzes the pixel intensity in the regions corresponding to the two goalposts. If the maximum intensity of a pixel is greater than the threshold intensity that the user defines, the program communicates with the DAQ board to switch the digital voltage channel which determines the polarity of the electrodes. This causes the electrodes to change polarity. The change in the polarity of the voltage causes the EOF to change directions in the pumping channels which results in the bead changing direction in the observation channel.

In order to provide additional flexibility during testing, the user can manually control the voltage across the electrodes in real time and can also manually switch the polarity of the electrodes. An additional feature of the μ-PONG system allows the user to record the video taken from the camera. When the video is recorded, an output file is also created with a time stamp for each frame of the video. Finally, the program also creates a file which contains the voltage, direction, and time-stamp whenever the polarity of the electrodes is reversed.

Results and Discussion:

Using μ-PONG, the motion of fluorescent beads can be controlled so that the bead moves between two goalposts. Figure 8 shows images of a bead as it travels between the goalposts.

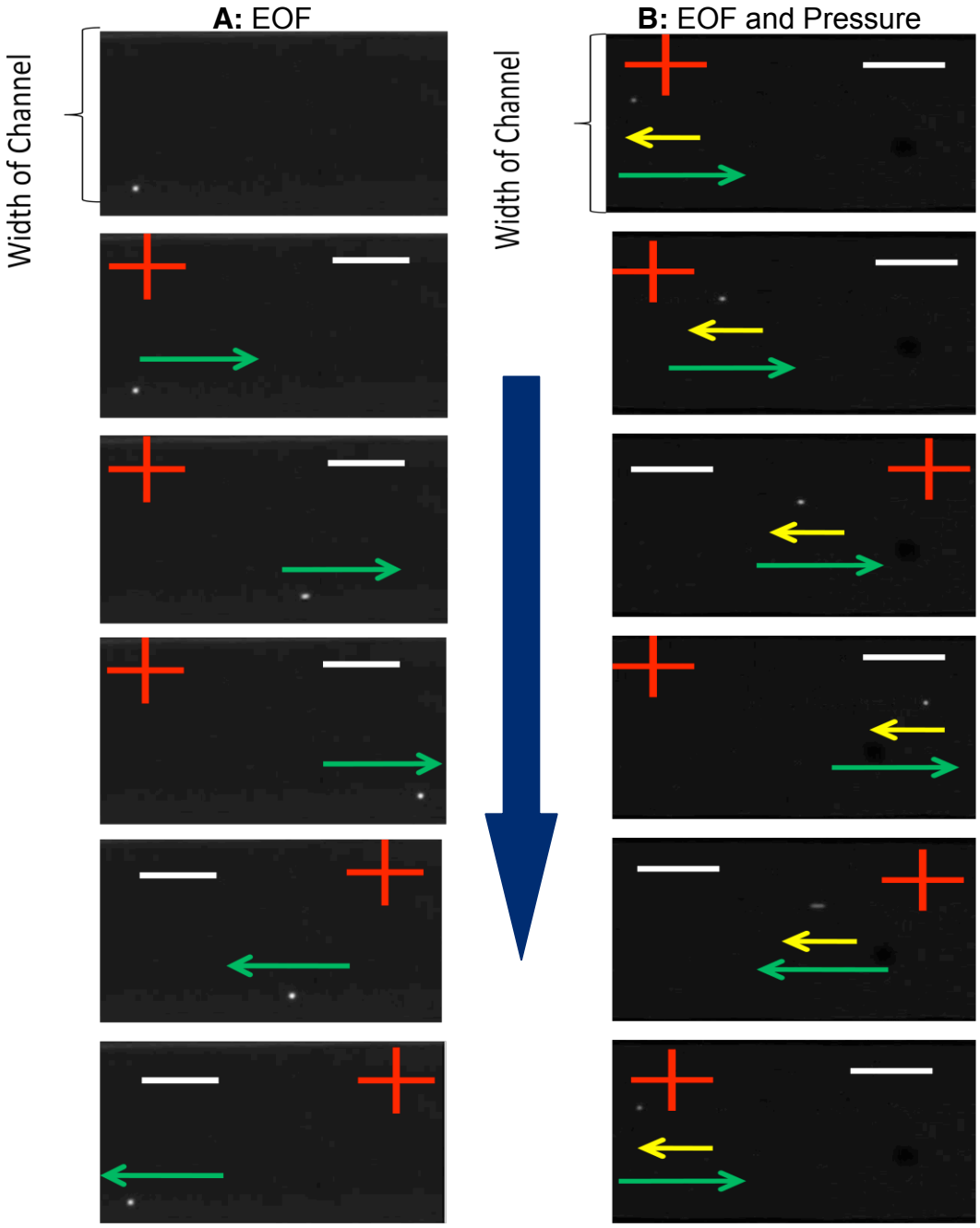

Figure 8. Images of fluorescent bead under EOF in the observation channel from two experiments. The white minus signs and the red plus signs represent the locations of the negative voltage electrode and the positive voltage electrode respectively. The green arrow shows the direction of the EOF in the pumping channels. The yellow arrow shows the direction of the pressure driven flow in the pumping channels. The blue arrow shows the progression of the frames with respect to time. **A)** Motion of a bead in a channel without an external pressure flow. The velocity is identical in both directions. **B)** Motion of a bead in a channel with an external pressure flow. The velocity is greater to the left. The stretching of the image of the bead while it travels to the left is a blurring effect caused by the shutter time of the camera.

When an external pressure flow exists, there is an asymmetry in the total flow rate in the device depending on the direction of the EOF. The asymmetry can be readily seen in graphs of the position and velocity of the bead as shown in Figure 9. The location of the bead is measured using an ImageJ program called MTrackJ. The position data for a bead are then combined with the timestamp. The average velocity of the bead between two frames of the video is found by dividing the change in the position of the bead by the time between the two frames.

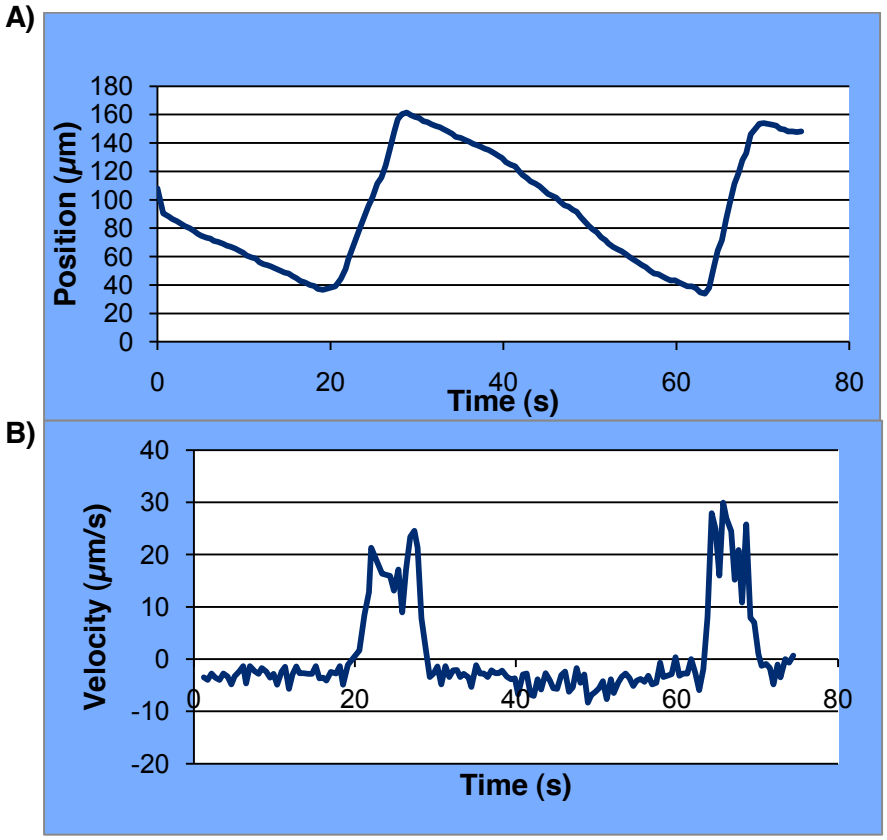

Figure 9. Position and velocity of a bead under both EOF and pressure flow. A) The position of the bead in μm with respect to the long axis of the channel is shown against the time. **B)** The velocity of the bead in μm/s is graphed against the time. The asymmetry in the positive and negative velocity confirms that there is a pressure flow acting on the pumping channels. Since the pressure flow does not change direction, the total velocity is larger in one direction. The graphs show that there is a large variation in the velocity as the bead moves through the channel. This makes the error in the average velocity large.

The large distribution could be caused from multiple factors. Other published experiments which measure the velocity in microfluidic channels have reported errors of 15-30% on the velocity measurements.[12] In addition, the μ-PONG software does not run smoothly (see Appendix B). The variation in time between frames in the program is accounted for in the timestamp, but there may still be an inherit inaccuracy due to our instrumentation. For beads with larger velocities, the image of the bead is elongated which can distort the position of the bead in the image. Finally, the bead's motion can be affected by multiple factors, especially influence by other particles in the fluid or near the surface of the channels. Though the velocity is variable in the short term, the beads do move in a uniform way over long distances.

The fact that μ-PONG can trap a bead enables prolonged data collecting of the velocity. The velocity can be averaged over the span of minutes with the same bead, instead of being forced to make a small number of measurements with one bead or combining the velocities of multiple beads. Since the pressure flow is dependent on the location of the bead in the channel, it is necessary for the beads to remain in the same area of the cross section of the channel. When the bead moves back and forth in the channel under the control of μ-PONG system, the bead remains relatively in the same position with respect to the walls as shown in Figure 10. Thus, the effect of the parabolic flow on making a measurement is reduced when one bead is used.

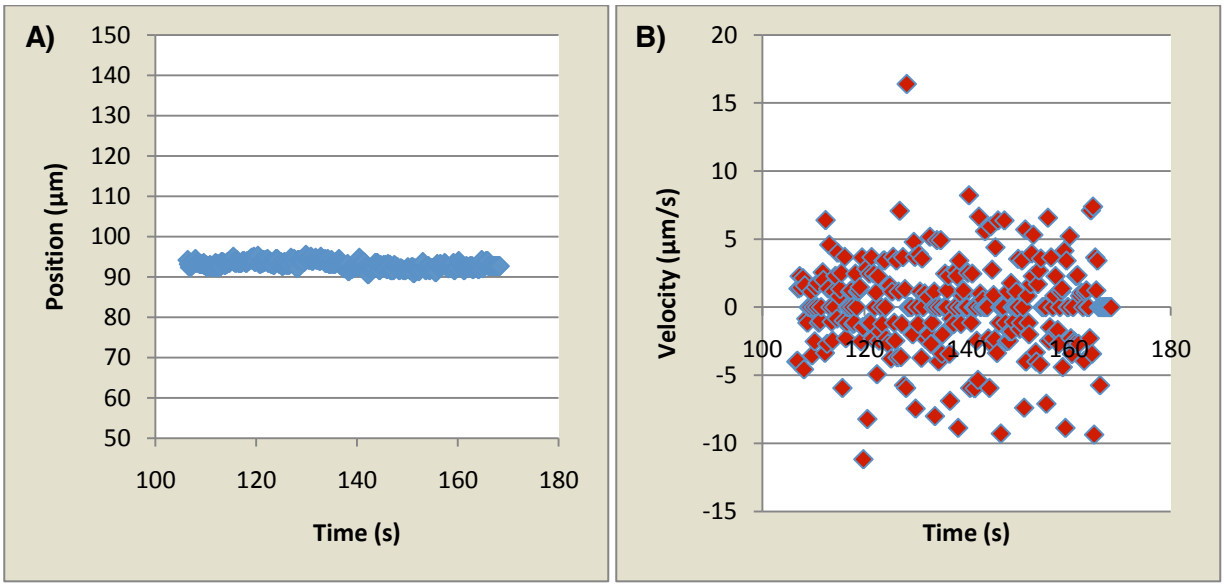

Figure 10. Motion of bead across the channel. A) The position of the bead with respect to the walls of the channel. There is a small drifting movement. **B)** The velocity of the bead relative to the walls of the channel. The average velocity of the bead is -0.05 μm/s with a standard deviation of 3μm/s. This shows that the bead undergoes random motion with a slight drift in one direction. The drift can be explained by the parabolic nature of the pressure flow.

In addition, the ability to obtain velocity data in both directions enables the velocity due to the EOF to be separated from the pressure-induced velocity. When the external pressure flow is always to the right, the total velocities are equal to

$$v_{left} = v_{pressure} - v_{eo} \quad (22)$$

$$v_{right} = v_{pressure} + v_{eo}. \quad (23)$$

By combining Eqs. 22 and 23, we can obtain the electroosmotic velocity

$$v_{eo} = \frac{(v_{right} - v_{left})}{2} \quad (24)$$

and the velocity component from the external pressure flow is

$$v_{pressure} = \frac{v_{right} + v_{left}}{2}. \quad (25)$$

Thus Eq. 24 can be used to find the EO velocity. The velocity due to the EOF in the observation channel is not the same as the v_{eo} in the pumping channels. The reason is the change in cross-sectional area of the pumping channels to the area of the observation channel. Thus, the results shown are only proportional to v_{eo}. With Eq. 24, the average velocities at different voltages for devices with 15 μm and 32 μm pumping channels were calculated. Figure 11 shows the results of the experiments.

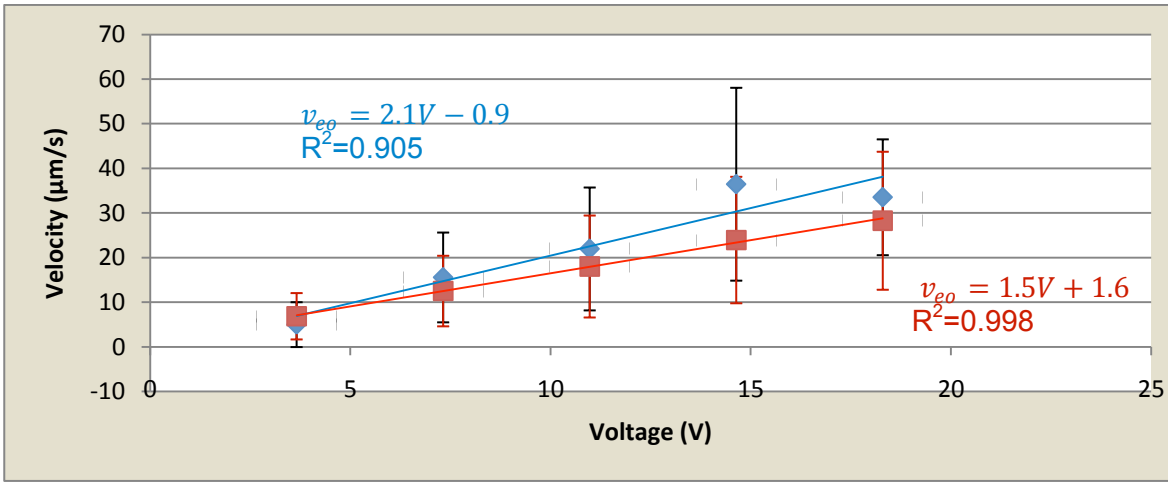

Figure 11. Comparison of the average EOF velocity of beads in devices with 15 *μ*m and 32 *μ*m channels. The red squares correspond to the velocity in a 32 μm pumping channel device, and the blue diamonds correspond to the 15 μm channels. The average velocity is proportional to the EOF by Eq. 24. The equation for the velocity for the 15 μm channels is $v_{eo} = 2.1V - 0.9$, with an R^2 value of 0.905. The equation for the velocity for the 32 μm channels is $v_{eo} = 1.5V + 1.6$ with an R^2 value of 0.998. The change in velocity with voltage is almost identical for the two types of devices.

Figure 11 shows that the EOF velocity of the beads in both geometries is almost identical. The large error in the velocity makes it impossible to tell the extent of the difference if any in the velocity for the different devices. This confirms that the pumping channels cannot be viewed as ideal EOF pumps obeying Eq. 6, and that the back pressure plays a vital role in the total flow rate.

In order to gain a better understanding of the backpressure in each device, the stalling pressure for the two types of devices was measured. The stalling pressure is the back pressure which balances with the EOF to produce no net flow.[12,13] To find the back pressure, two glass pipettes were attached to the end wells of the devices. The pipettes had an outer diameter of 2 mm and an inner diameter of 1mm. A potential difference was applied to the device in one direction so that the EOF moved water to one of the pipettes. As the water level increased in one of the pipettes, the external pressure flow increased. The height of the water stabilizes once the pressure flow balances the EOF. By measuring the difference in the height of water in each channel, the pressure was calculated. The pressure flow, found using Eq. 12, is equal to the EOF. Capillary forces and evaporation made accurate measurements of the height of the water difficult. To increase the EOF force compared to the capillary forces, the device was connected to a potential source set at 40 V. The formula used to calculate the stalling pressure is

$$\Delta p = \rho g \Delta h \tag{26}$$

where ρ is the density of water, g is the acceleration due to gravity and Δh is the difference in the height of the water in the two pipettes. Table 1 shows the results of the back pressure experiments.

Table 1: Stalling Pressure

Device	Change in Height(mm)	Stalling Pressure (Pa)	Expected Flow Rate ($\mu m^3/s$)
15	3.2±0.4	31±3	$6.2\times10^5\pm0.6\times10^5$
32	1.6±0.4	16±3	$3.4\times10^5\pm0.6\times10^5$

The stalling pressure for the device with 15 μm channels is almost twice the stalling pressure for the device with 32 μm channels. This corresponds to a greater flow rate for the 15 μm device than the 32 μm device. The 15 μm pumping channels have a much larger resistance than the 32 μm channels. In fact, the resistance in the 32 μm channel device is dominated by the resistance of the observation channel. As a result, the smaller pumping channels are able to resist a greater external pressure, not because they create a greater EOF, but because they reduce the pressure flow and hence are efficient.

The device has an intrinsic asymmetry caused by the glass slide surface. Glass and PDMS will have unique Zeta potentials which could cause the EOF to be different at different walls of the pumping channels. The Zeta potential depends on both the charges of the surface and the concentration of ions in the fluid. Experimentally, the Zeta potentials of glass and PDMS have been found to be similar.[14,15] Still, the difference could cause a gradient in EOF in the vertical direction and affect the total flow from the pumping channels. Experiments were performed to compare the EOF velocity of the bead in a device with one glass side compared to a device with only PDMS slides. The results are shown in Figure 12.

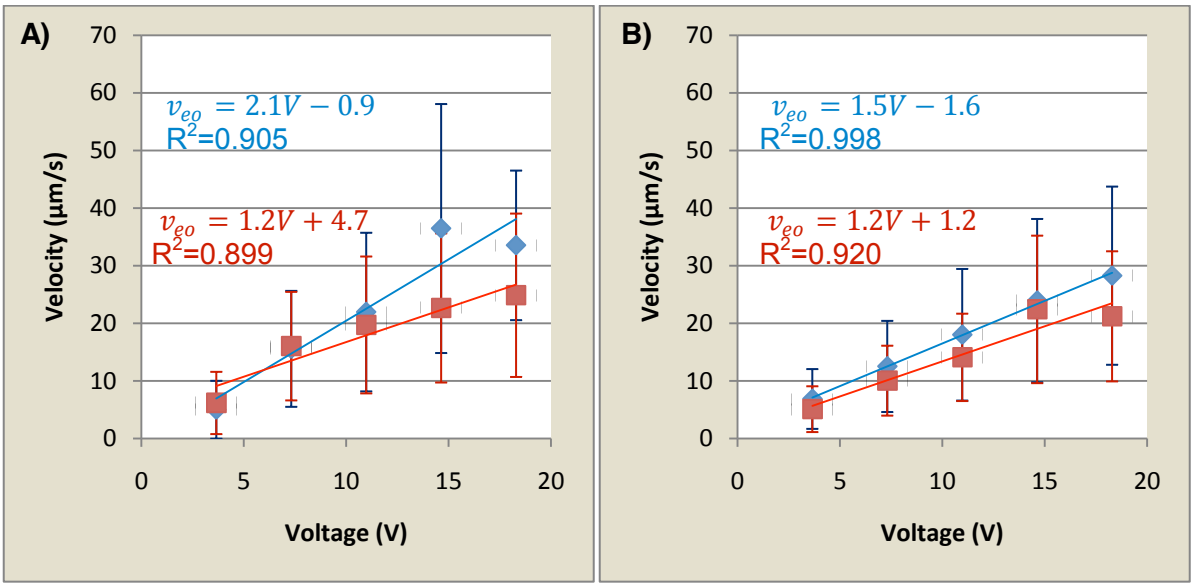

Figure 12. Velocity for devices with PDMS and glass floors. The red squares correspond to the device with all four sides made of PDMS. Blue diamonds correspond to channels which have glass bottom surfaces. **A)** The device has pumping channels of 15 μm. The Red (PDMS) velocity as a function of voltage is $v = 1.2V + 4.7$ with an R^2 value of 0.899. The Blue (glass) velocity changes as a function of voltage by the equation $v = 2.1V - 0.9$ with an R^2 value of 0.905. **B)** The device has pumping channels of 32 μm. For Red (PDMS), the velocity as a function of voltage is $v = 1.2V + 1.2$ with an R^2 of 0.920. For Blue (glass), the velocity as a function of voltage is $v = 1.5V + 1.6$ with an R^2 of 0.998.

There is little difference between the EOF velocity for the devices with a glass slide and the devices with only PDMS sides compared with the error in calculating the velocity. This corresponds with the similarity in the distilled water Zeta potentials for glass and for PDMS.

Another possible effect is decay of the EOF with time. It is possible for the EOF to decay with time as the surface charge is reduced which reduces the number of ions in the EDL. Each device was used in multiple consecutive experiments, normally lasting for 10 to 15 minutes. For some experiments, the device could be used for an hour. All experiments that were done on one device took at least an hour, and it is important to investigate any possible changes in the flow rate with time. In order to gain a better understanding of how the flow rate changes with time, experiments were performed to monitor decay of the EOF velocity with time. A device was fabricated and connected to PONG as with a normal experiment. Once a bead was trapped in the device, the velocity was monitored for a couple of minutes. After an hour, another measurement of the velocity was taken. The process was repeated for the first five hours after the device had been bonded. After five hours, the device was placed in a covered dish with Kimwipes that were saturated with distilled water. The next day (24 hours after the device had been fabricated), the device was reconnected to PONG and more measurements were taken. Though evaporation did occur in the wells, the channels were still filled with water. For each day's measurements, the wells were completely refilled and new beads were placed in the device. Figure 13 shows the results of the velocity at different times.

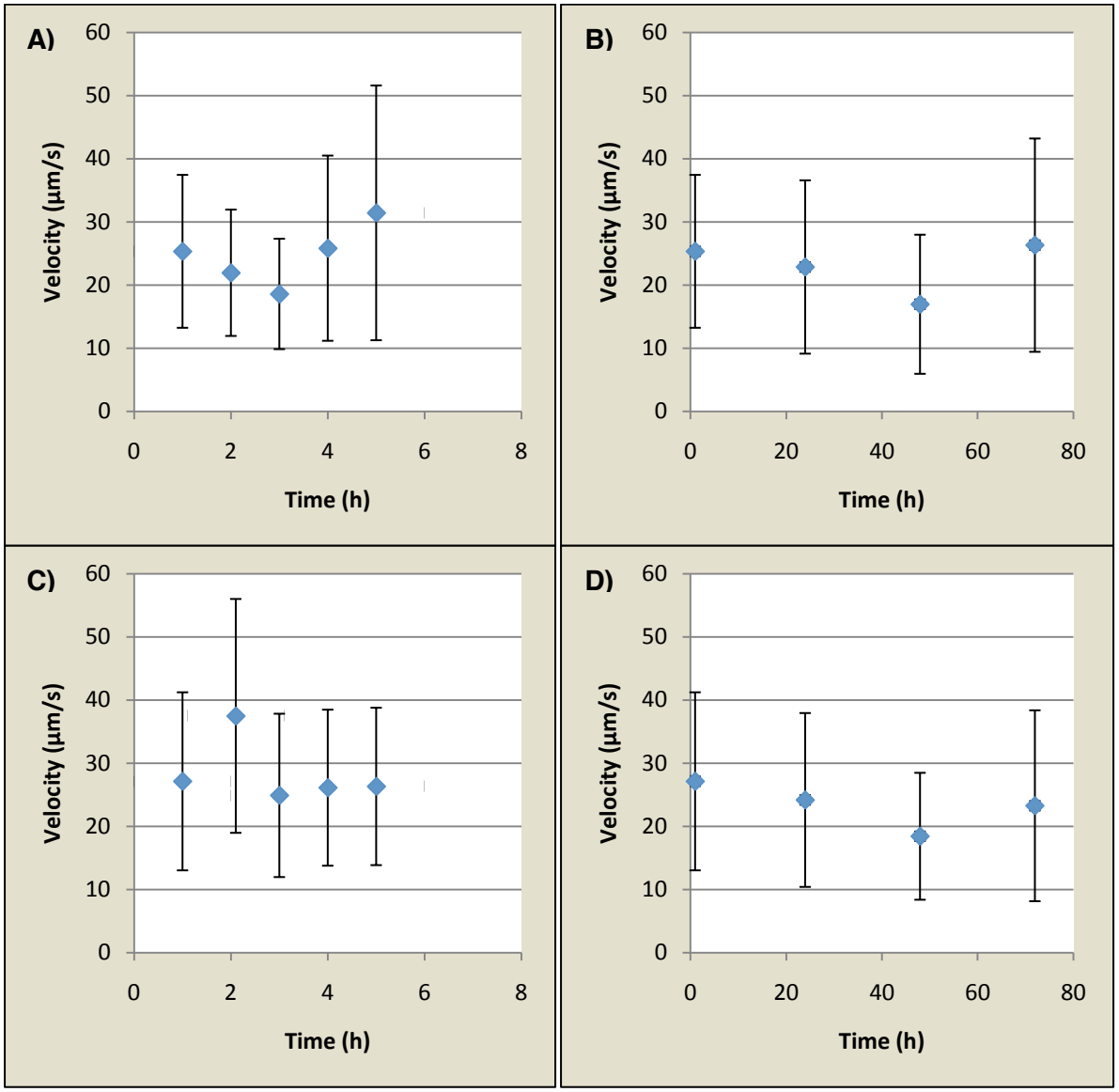

Figure 13. Change in EOF with time. A) The average velocity of a bead in a device with 32 µm channels while 4 V was supplied to the device for 5 hours. **B)** The average velocity of a bead in a device with 32 µm channels over 72 hours. **C)** The average velocity of a bead in a device with 15 µm channels while 4 V was supplied to the device for 5 hours. **D)** The average velocity of a bead in a device with 15 µm channels over 72 hours.

As the figure shows, if there is any decay in the EOF with time, it is minimal, especially compared with the error in the velocities. The device can be run over multiple hours without skewing the results.

Since EOF is a plug flow, it is impossible for EOF to completely cancel a pressure flow everywhere across a channel in which EOF and pressure flows are both present. Still, it is possible for the net flow through a pumping channel to be zero which occurs when the external pressure equals the stalling pressure.[12,13] As a result, it is possible for there to be no net flow in the observation channel when the EOF balances the pressure flow in the pumping channels. Since the pressure flow is greatest at the center of the device, the flow in the center is in the direction of the pressure flow, while the flow adjacent to charged walls is dominated by the EOF. Figure 14 shows the result of balancing the EOF and the pressure flow in the pumping channels.

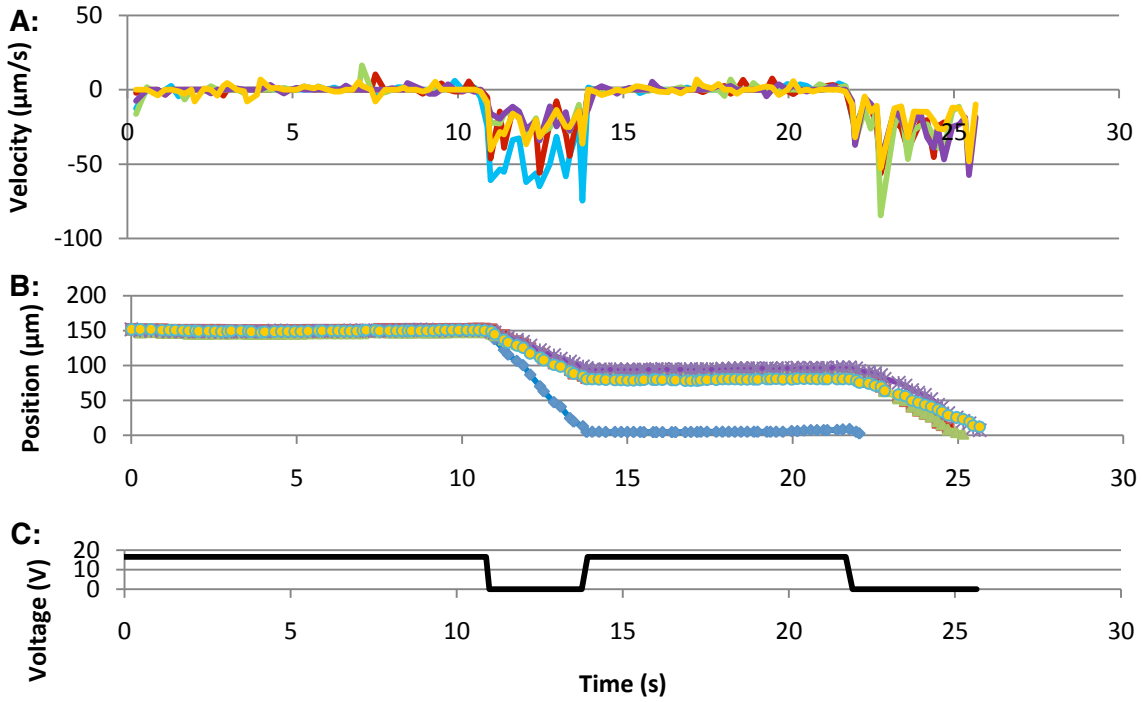

Figure 14. Effect of Balancing Pressure Flow with EOF in Pumping Channels as measured by the motion of multiple beads. The voltage difference between the electrodes was calibrated so that the EOF flow would balance the pressure flow in the channels resulting in no net flow. **A)** The position of the bead versus the time. The positions of the beads were normalized so that they all appear to start at the same position. The beads are all at different positions along the width of the channel. The blue line is for a bead 10 µm from the far side of the channel. The red line is for a bead 23 µm from the side of the channel. The green line is for a bead that is 38 µm from the far side of the channel. The purple line is for a bead 67 µm from the far side of the channel. The orange line is for a bead 87 µm from the far side of the channel. **B)** The velocity of the beads versus time. The graph shows that the velocity of the beads fluctuates around zero when the EOF is present in the pumping channels. **C)** The expected voltage across the electrodes versus time.

Future Directions:

As seen in the results, one troubling aspect of the experiments performed with µ-PONG is the large variation in the observed velocity of the bead. This may be due to the fact that the bead may move in the vertical direction within the channel and hence experience different forces due to the nature of the parabolic distribution of the fluid velocity within the channel.

In order to gain a better understanding of the three-dimensional bead motion in the observation channels, a method needs to be developed to show the vertical position of beads in the device in real time. This can be accomplished by analyzing the amount of defocusing on the bead.[16] Another way to gain information about the height of the bead is to use a single mirror that is inserted into the device to create a virtual image of the vertical plane that appears next to the horizontal image of the channel as shown in Figure 15.[17]

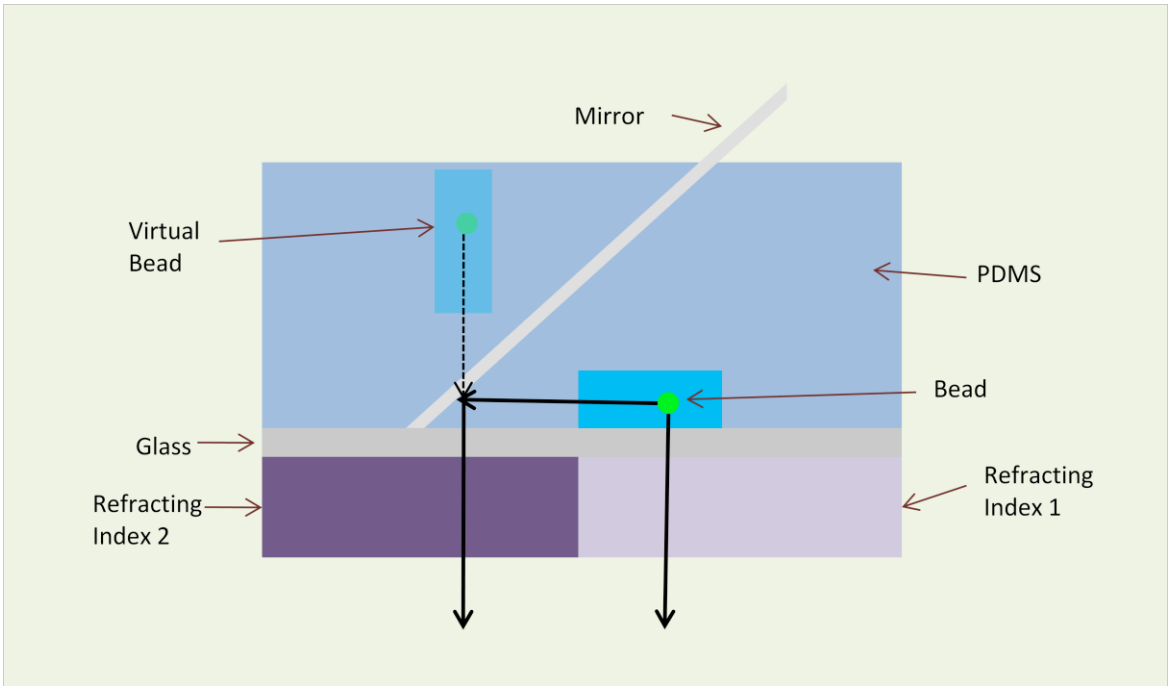

Figure 15. Diagram of 3D Imaging Mirror. The figure shows how a mirror can be used to gain information about the vertical position of a bead. The mirror creates a virtual image of the bead in which the image has been rotated 90 degrees from the real image. In order to get both the virtual and real images to be in focus at the same time, the two images must pass through materials with different indices of refraction.

A mirror positioned at an angle of 45 degrees with respect to the bottom of the device will create a virtual image as shown in Figure 16.

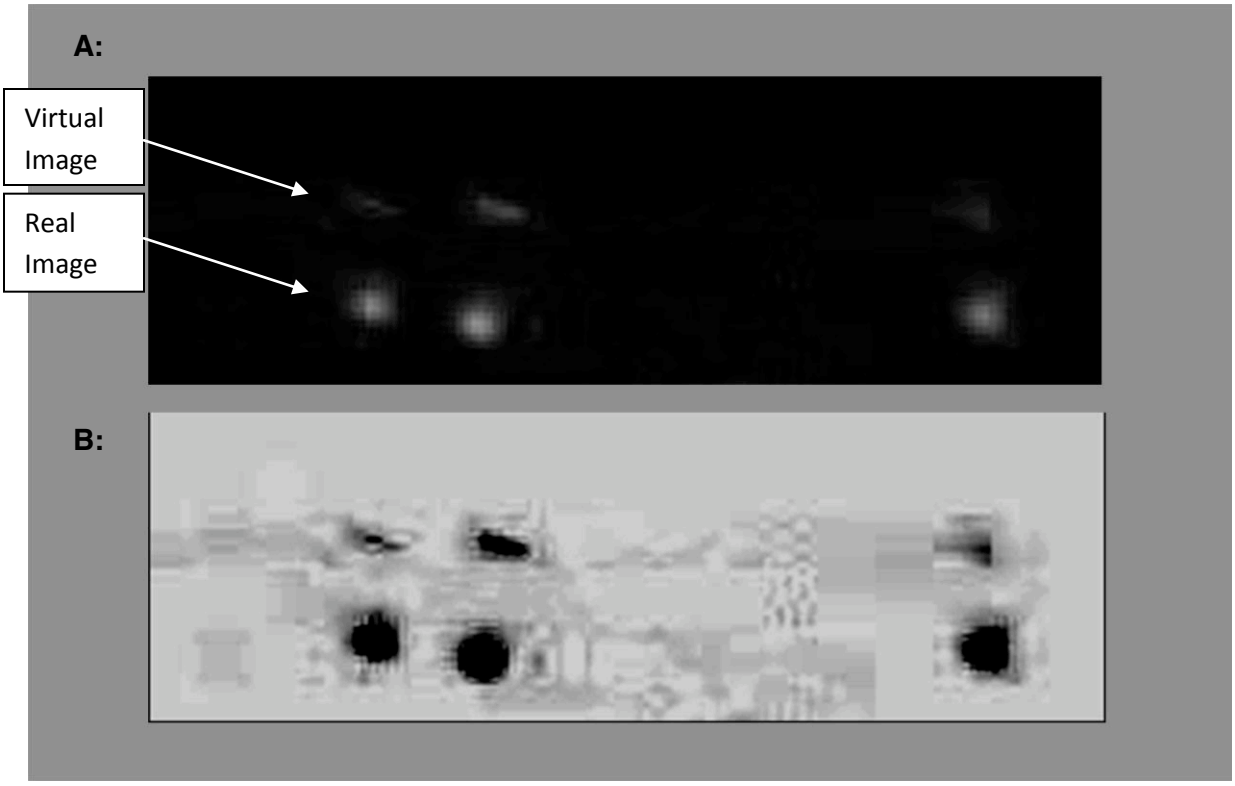

Figure 15. Defocused real and virtual images of beads created by the mirror. In order to see both images at the same time, the focus of the microscope was positioned between the focal plane of the real and virtual beads so that both images were out of focus to a certain degree. The virtual beads are also distorted because of the warping of the mirror at the glass surface. This can be reduced by setting the mirror in a PDMS channel during the fabrication process. **A)** The regular image of the beads. **B)** The colors have been inverted, and the contrast has been increased in order to better see the virtual beads.

There is an intrinsic problem with obtaining simultaneous focus in the real (XY) plane and the virtual (XZ) plane using this category of mirrored device. The virtual image of the bead is at a higher vertical distance than the actual bead. Thus, the optical path length of the virtual image needs to be modulated so that both images can be in focus without changing the lens of the microscope. Choi *et al.* showed that the placement of a glass slide under the position of the virtual image but not under the real image enables both images to be focused at the same plane. The thickness of the slide, *t*, needs to be

$$t = \frac{n_{PDMS}}{n_{glass} - n_{air}} d \tag{27}$$

where n_{PDMS}, n_{glass}, *and* n_{air} are the indices of refraction for PDMS, glass, and air respectively and *d* is the distance of the channel to the mirror. The equation holds for any change in the index of refraction for two medium.

The difficulty with Choi's apparatus is the placement of the glass slide. Therefore, we looked into using liquid crystals to modulate the path length. Some liquid crystals have the property of changing the index of refraction through them when exposed to an electric field. We

propose that by alternating the electric field, we can change between two indexes of refraction and therefore alternate the focus between the real and virtual planes.

On another topic, additional work to characterize the behavior of our multi-parallel channel EOF pumps should include studies to investigate performance of devices loaded with different fluids, especially fluids such as cell culture media. Initial tests using a Ringer' solution revealed a dramatic increase in beads sticking to the side of the channel, possibly due to some sort of electrostatic attraction.

Conclusions:

We developed a device in which a hydrostatic pressure force can be balanced by an opposing EOF dynamically produced in an array of parallel pumping channels such that there is no net flow in the pumping channels. When there is no net flow in the pumping channels, there is no flow (regardless of position in the channel) in the channels that are connected in series with the pumping channels which are outside the effect of the electric field created by the electrodes. This result demonstrates that μ-PONG and the device designs we investigated could be incorporated into a more complex microfluidic system that requires the ability to modulate the flow or create "stop flow" in channels.

The results of the bead velocity experiments show that in the two device designs which were examined, there was a small but rather insignificant difference in the flow rates that are produced by the 15 μm and 32 μm pumping channels under circumstances where hydrostatic pressure heads were not large. Although the 32 μm channel array should theoretically produce a larger EOF than the 15 μm channel array (due to the larger channel volumes associated with the 32 μm device), this would only be true under conditions of no back pressure. In the actual experimental conditions, the back pressure due to restrictive channel dimensions was not negligible, and thus the superior ability of the smaller 15 μm channel array to resist pressure flow, compensated for its lower theoretical (no back pressure) pump rate. The ability of the device with smaller pumping channels to balance a greater external pressure was verified with stalling pressure measurements.

The experiments undertaken in this study demonstrate that the μ-PONG instrumentation system can be used to investigate the effects of a variety of parameters on EOF. Among the parameters investigated as part of this study are the efficacy of PDMS versus glass in production EOF and the time related decay rate of EOF in PDMS devices as the PDMS ages. These results give a better understanding of the properties of EOF which will be useful in designing devices that incorporate EOF in the future.

References:

1) F.F. Reuss. "Sur un nouvel effet de l'electricite galvanique," Memoires de la Societe Imperiale des Naturalistes de Moscou **2**, 327 (1809)
2) HLF von Helmholtz. "Studien uber electrische grenzschichten," Ann Phys **7**, 337 (1879).
3) M.V. Smoluchowski. "*Versuch einer mathematischen theorie der koagulationskinetik kolloider losungen*," Z Phys Chem **92**, 129 (1917).
4) X. Wang, C. Cheng, S. Wang, S. Liu. "Electroosmotic pumps and their applications in microfluidi systems," Microfluid Nanofluid **6**, 145 (2009).
5) A. E. Cohen and W. E. Moerner. "Internal mechanical response of a polymer in solution," Physical Review Letters **98**, 116001 (2007).
6) L. Cui, D. Holmes and H. Morgan. "The dielectrophoretic levitation and separation of latex beads in microchips," Electrophoresis **22**, 3893 (2001).
7) S. K. Sia and G. M. Whitesides. "Microfluidic devices based on poly(dimethysiloxane) for biological studies," Electrophoresis **24**, 3563 (2003).
8) M.A. Eddings, M.A. Johnson, and B.K.Gale. "Determining the optimal PDMS-PDMS bonding technique for microfluidic devices," J. Micromech. Microeng. **18**, 067001 (2008).
9) W. Hellmich, J. Regtmeier, T. T. Duong, R. Ros, D. Anselmetti, and A. Ros. "Poly(oxyethylene) Based Surface Coatings for Poly(dimethylsiloxane) Microchannels," Langmuir **21**, 7551 (2005).
10) G. B. Lee, C. H. Lin, K. H. Lee, and Y. F. Lin. "On the surface modification of microchannels for microcapillary electrophoresis chips," Electrophoresis **26**, 4616 (2005).
11) S. Liu, Q Pu, and J Lu. "Electric field-decoupled electroosmotic pump for microfluidic devices," Journal of Chromatography A, **1013,** 57 (2003).
12) A. Brask, G. Goranovic, and H. Bruus. *Theoretical analysis of the low-voltage cascade electro-osmotic pump.* Sensors and Actuators B **92**, (2003).
13) D. G. Yan, C. Yang, X. Y. Huang. *Effect of finite reservoir size on electroosmotic flow in microchannels.* Microfluid Nanofluid **3**, 333 (2007).
14) A. Sze, D. Erickson, L. Ren, and D. Li. "Zeta-potential measurement using the Smoluchowski equation and the slope of the current-time relationship in electroosmotic flow," Colloid and Interface Science **261** (2003).
15) V. Tandon, S. K. Bhagavatula, W. C. Nelson, B. J. Kirby. "Zeta potential and electroosmotic mobility in microfluidic devices fabricated from hydrophobic polymers: 1. The origins of charge," Electrophoresis **29**, 1092 (2008).
16) B. Rohrman. *Micro Programmable Object Navigation Gadget (µ-PONG) for Studying Electroosmotic Flow ion a PDMS Microchannel*. Senior Honors Thesis, Vanderbilt University, (2009). http://hdl.handle.net/1803/2950.
17) S. Choi, S. Kim, J. Park. "Optical path-length modulation for three-dimensional particle measurement in mirror-embedded microchannels," Lab Chip **10**, 335 (2010).

Acknowledgements:

I am grateful to Phil Samson, Dmitry Markov, and John Wikswo for their guidance and assistance throughout the project. I would also like to acknowledge Brittany Rohrman whose work on μ-PONG paved the way for my own work. I would like to acknowledge Allison Price for her help with proofreading. In addition, I would like to acknowledge the members of the Vanderbilt Institute for Integrative Biosystems Research and Education (VIIBRE) and the Searle Systems Biology and Bioengineering Undergraduate Research Experience (SyBBURE) for their assistance. I thank my family and friends for their support. Finally, I acknowledge funding support from the William A. and Nancy F. McMinn Foundation and the National Science Foundation grant DMR-0619789.

In addition, I would like to thank Charles Brau, Shane Hutson, and Kevin Seale for serving on my committee of independent examiners.

Appendix A:

Figure 17: LabVIEW Block Diagram

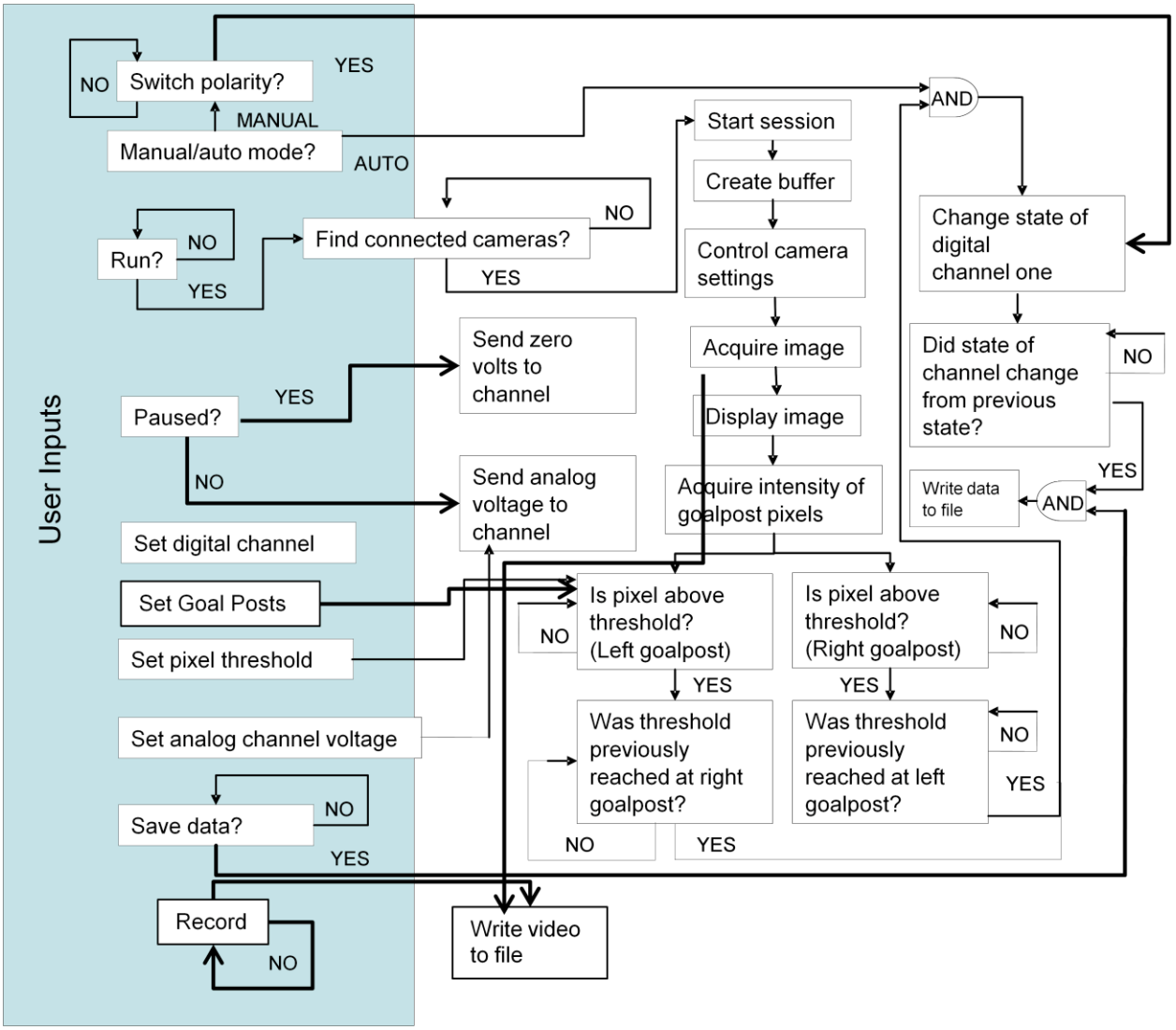

Appendix B:

Figure 18: Histogram of the Time between Frames of Video for *μ*-PONG

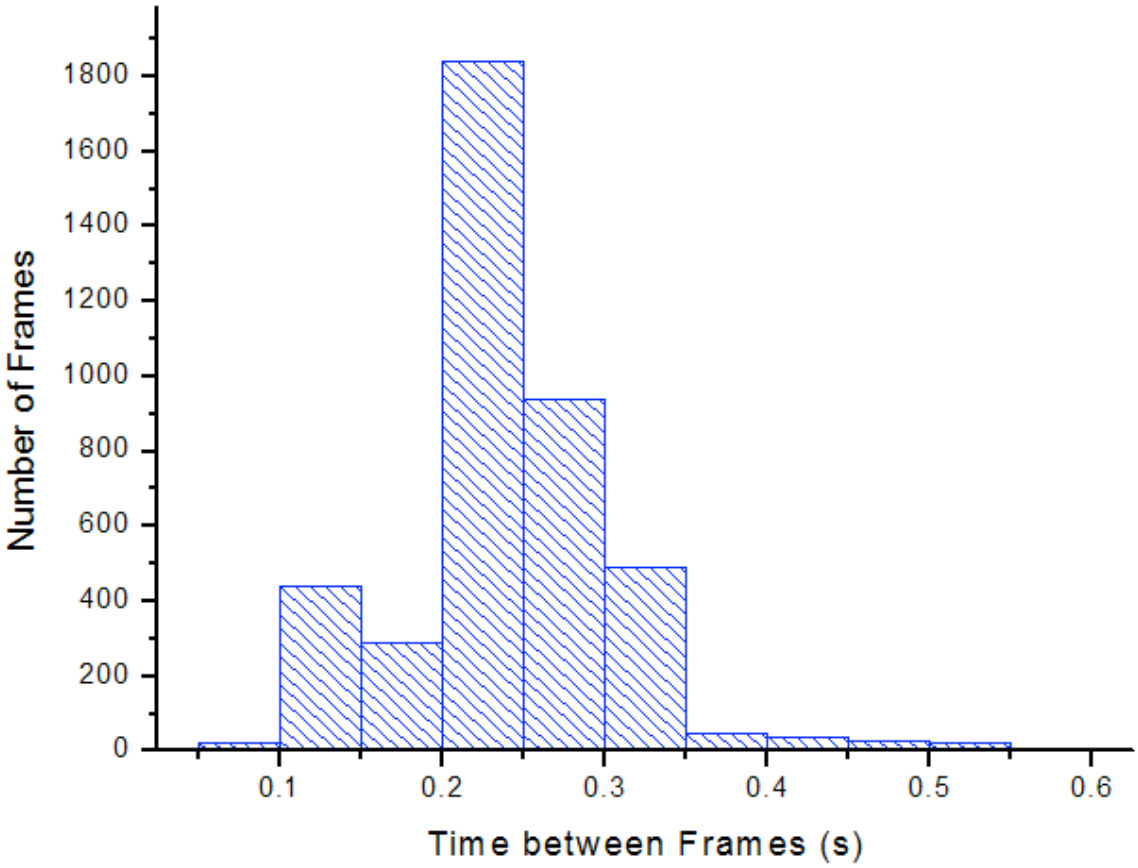

The histogram shows the distribution of the amount of time between two frames of a video produced by μ-PONG. The average time between frames is 0.24±00.07s. This corresponds to a frame rate of 4±1fps. Ideally, the video should run at 10 fps. The distribution might explain the large error in calculating the velocity.

Appendix C: Voltage Output of μ-PONG

Table 2: Voltage across Electrodes for Input Voltage

Input Voltage (V)	Expected Output Voltage (V)	Actual Output Voltage
1	3.66	3.81
2	7.32	7.62
3	10.98	11.44
4	14.64	15.24
5	18.30	19.04

Appendix D: Calculating the Position and Velocity of a Bead

The LabView program MTrackJ was used to find the position of the beads. LabView converts the video file into a Tiff stack. MTrackJ requires the user to manually click on the position (in pixels) of the bead. Once the user clicks on the frame, the program records the x- and y- position of the bead as well as the frame. The program then switches to the next frame in the stack of images. After the position of the bead is recorded for each image in the stack, the position of the bead for each frame is outputted into a *.dat file. The data are then manipulated using a spreadsheet program (Excel). The position of the bead is converted from pixels to μm. For the experiments, each pixel corresponded to 0.5 μm. The time of each frame is then taken from the timestamp file and combined with the position data. The average velocity between frames is calculated using the standard equation

$$v = \frac{x_2 - x_1}{t_2 - t_1} \tag{28}$$

In order to calculate the average velocity using Eq. 24, the data were grouped into two sets, the velocity to the right, and the velocity to the left. The velocity when the bead was beyond either goalpost was ignored because there were areas where the EOF should be changing direction and therefore the bead would be changing direction as well. The average of the left velocity and the average of the right velocity were found. Then v_{eo} was found using Eq. 24.